A Multi-Criteria Approach to Electro-Mechanical Actuator Selection in Non-Road Mobile Machines

Matias Alenius*, Vili Vironmäki, Vinay Partap Singh, Tatiana Minav

Faculty of Engineering and Natural Sciences, Tampere University, Tampere, Finland
* Corresponding Author: matias.alenius@tuni.fi

Abstract

The electrification of non-road mobile machines has gained momentum due to tightening emissions regulations. However, linear actuating systems in these machines often remain hydraulic, despite advancements in electro-mechanical actuators (EMAs), which offer benefits such as improved energy efficiency, controllability, and noise reduction. Selecting EMA for diverse applications involves complex trade-offs, requiring detailed simulations that can increase time-to-market. To address this, a novel EMA selection tool has been developed, incorporating a scaling algorithm to adjust operating points for lower force and velocity constraints. The tool evaluates EMA alternatives based on productivity, size and cost using a multi attribute decision-making approach, supported by a modified analytic hierarchy process to weight design criteria. The tool is tested on two non-road mobile machines—an excavator, and a forest forwarder—using duty cycle data generated using the co-simulation models based on Mevea and Matlab/Simulink simulation environments. This structured approach aims to streamline EMA selection, accelerate electrification adoption, and promote sustainable solutions in non-road mobile machines.

Keywords: Electro-mechanical actuators, Multi-attribute decision-making, Non-road mobile machines, Actuator selection, Design objectives

1 Introduction

Non-Road Mobile Machines (NRMMs) contain a large variety of machines used for different applications such as construction, forestry, agriculture, and mining, to name a few. These machines usually have application-specific linear actuation systems, which have requirements that are dependent on the specific application or purpose of the system. The differing requirements imposed on the linear actuators, including energy efficiency, cost, accuracy, size, productivity, and thermal behavior, vary greatly between applications, and the requirements are often conflicting. Thus, there does not exist a single actuation system that fits all NRMMs, and the designing of linear actuating systems involves trade-offs between the requirements.

Environmental concerns and economic factors have heightened the demand for energy efficiency, as valve-controlled hydraulics, which are frequently used, often operate with low efficiency [1]. In the literature, a large variety of technologies have been proposed to be used in the linear actuators of NRMMs [2]. Individually powered actuator concepts such as Electro-mechanical Actuator– (EMA) [3, 4] and Electro-hydrostatic Actuators (EHA) [5] have shown significant improvements in energy efficiency compared to their conventional hydraulic counterparts. However, the integrated nature of such actuators means that the power needed for the actuator's actions needs to be generated by the connected electric motor, unlike in centrally powered actuating systems, where power generated by the prime mover can be distributed flexibly to any actuator. Local power generation leads to higher total installed power, if similar peak productivity is required from every actuator in multi-actuator system. Additionally, the use of fixed transmission ratios in individually powered actuators restricts the velocity range, where the actuator can reach its maximum power, thus limiting further the plausible region of operation [6].

The total installed power needs to be kept at levels that do not make the systems economically inaccessible; hence, a compromise must be made with the peak power capacity of individual actuators. This compromise shall be made in a way that the productivity and cost of the machine are acceptable for the end user. The dimensioning of the actuator and its components therefore has multiple conflicting objectives. For example, actuator costs, size, and productivity, all of which cannot be minimized simultaneously, making the

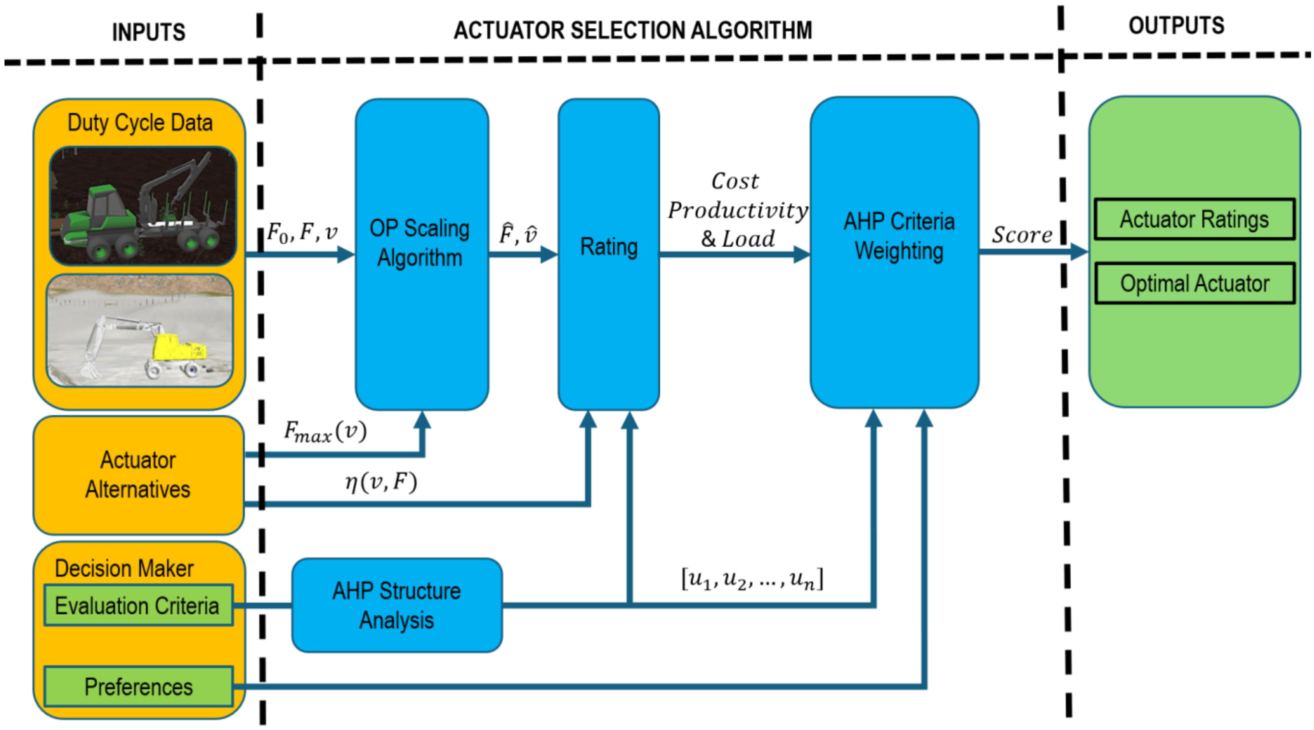

Figure 1: Overview of the actuator selection process

dimensioning problem a Multi-Objective Optimization (MOO) problem with conflicting objectives.

Multi-objective optimization methods have been widely used for integrated hybrid vehicle drivetrain topology, and component and control optimization [7, 8, 9] in both the automotive industry and for NRMMs. However, the integrated system and control design using dynamic simulations and MOO require expertise in modelling, model integration, and simulations in multiple fields, which is time-consuming [10]. The problems of the integrated MOO approach are amplified by the increased search space of possible solutions and the multi-DOF nature of manipulators driven by linear actuators. Additionally, the lack of standard duty cycles used for the simulations may lead to optimizing the linear actuators for conditions different from real world operating conditions [11]. Xue et al. [12] have used simulation-based parameter search for Pareto optimal solutions using multi-objective particle swarm optimization, though no selection method is used there. The actuator selection problem is formulated so that predefined selection of actuators is compared, thus the use of more general MOO methods is not necessary as all possible combinations can be evaluated, thus eliminating the need to find the Pareto optimal set. The scope of the said study is to develop methods to structure the decision-making process. Multi-Attribute Decision Making (MADM) methods have been applied to dimensioning and selection of components in many fields [13, 14]; however, these methods rely on low-resolution metrics to rate the alternatives. Fassbender et. al. [15] presents a broad evaluation algorithm for actuator technology selection in heavy-duty mobile machines, which again relies on subjective low resolution rating scales and the expertise of the designer rating the alternatives. Yu et al. [16] used MOO methods to generate Pareto frontier and Analytic Hierarchy Process (AHP), a method to systemize and solve MADM problems [17], to choose the optimal design for EHA to be used in aeronautical environment. However, the approach cannot be used to evaluate the productivity of the actuator as the load torque and velocity of the actuator during the duty cycle are considered as known design parameters. An exhaustive search for optimal hydraulic system topology is used by Jiao et al. [18] for aircraft control actuation system selection using MOO and AHP. Nonetheless, the said study focuses on the safety of the system and the metrics used for selection are not capable of evaluating productivity of actuator accurately, as the duty cycle is a fixed design parameter.

Considerable research has been conducted for the traction system optimization of hybrid-electric vehicles. Whereas similar optimization methods have been studied to a lesser extent for design parameter optimization of linear actuators. Moreover, the system-level optimization and decision-making frameworks for selecting linear actuators in NRMM have not been presented.

The present paper bridges this research gap for the selection of distributed linear actuating systems in NRMM applications, where trade-offs between systems productivity and other performance metrics are assessed without using high-order models. This paper aims to present a measurement data-driven multi-criteria approach selection framework that aids in the selection of EMAs to match the power demand in a predetermined duty cycle to actuators' power output capacity.

Figure 1 shows the overview of the proposed actuator selection process described in this study. An MADM algorithm based on AHP, and a novel operation point scaling algorithm is proposed to find the optimal trade-offs between productivity and other selection criteria. The developed OP scaling algorithm based on reduced order model of the system to predict EMA alternatives' OPs for recorded duty cycle is presented. The framework is then used for selecting EMAs for two different NRMM a forest forwarder and an excavator using duty cycle data recorded from detailed co-simulation models of the machines. The use of the selection algorithm is described in detail with example use case of the forest forwarder.

The next sections present the details about the use case machines and their modeling and simulation. The third section presents the algorithms used in this study and an example use case for the EMA selection algorithm, selecting forest forwarders' lift and tilt cylinders. In the fourth chapter, the results for the presented example use case of the forest forwarder and excavator are presented, with concluding remarks and future prospects at the end.

2 Simulation models of the non-road mobile machinery

The data for the operation points used in the study is generated using co-simulation models of the two use-case NRMMs: a forest forwarder and an excavator. The multibody dynamics models of the said machines are prepared in the Mevea modeling environment, while the models of EMA are made in MATLAB/Simulink and validated through experimental data. Mevea is a digital twin technology and simulation platform featuring its own physics engine, which models the mechanics, hydraulics, power transmission, and operating environment of machines [19].

The communication between MATLAB/Simulink and Mevea software is established using a socket interface provided by Mevea [20]. This interface leverages the TCP/IP protocol to facilitate synchronous data transfer between Mevea and Simulink models at predetermined time intervals. The following sub-sections elaborate more on individual machine case models and the EMA model, respectively.

2.1 Use case NRMM

2.1.1 Forest Forwarder

A forest forwarder is an articulated NRMM used in logging operations to transport logs from the harvesting site to a roadside landing. It is equipped with a hydraulic crane and grapple for loading and unloading logs, along with lift and tilt mechanisms for precise handling. The conventional forwarders are equipped with Load-Sensing (LS) hydraulics, and the control of the linear hydraulic actuators is achieved using the throttling principles of hydraulic valves. The lift and tilt actuators are the most power-intensive ones among all others, consuming the majority of the power delivered by centralized LS hydraulics [21]. Hence, this study focuses on these two actuators, replacing them with EMA. The system shown in fig. 2 employs EMAs as lift and tilt actuators, while the rest of the system operates using LS hydraulics.

A log lifting and loading cycle is considered for further investigation, as this represents the most common operation of a forest forwarder. Figure 3 shows the lifting cycle used in the study where actuator position and forces are plotted. Initially, the boom is in a standby position, and a log of 250 kg is positioned 7 meters away from the boom's pillar, and the forwarder's load space is empty. During the cycle, the log is lifted from the ground and loaded into the load space of the forwarder machine, and the boom goes back to its initial position.

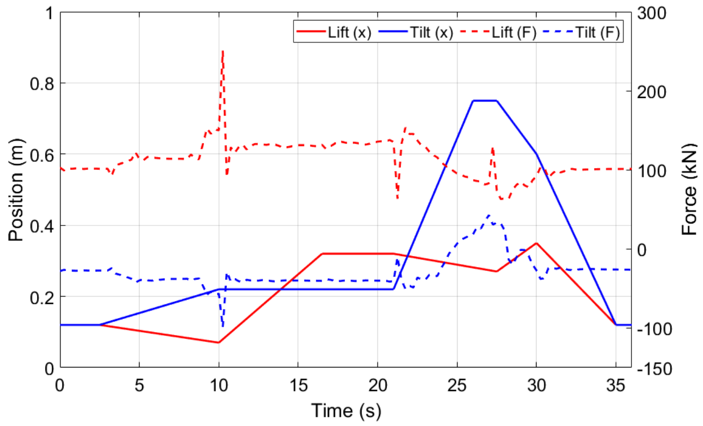

Figure 3: Duty cycle for the forest forwarder

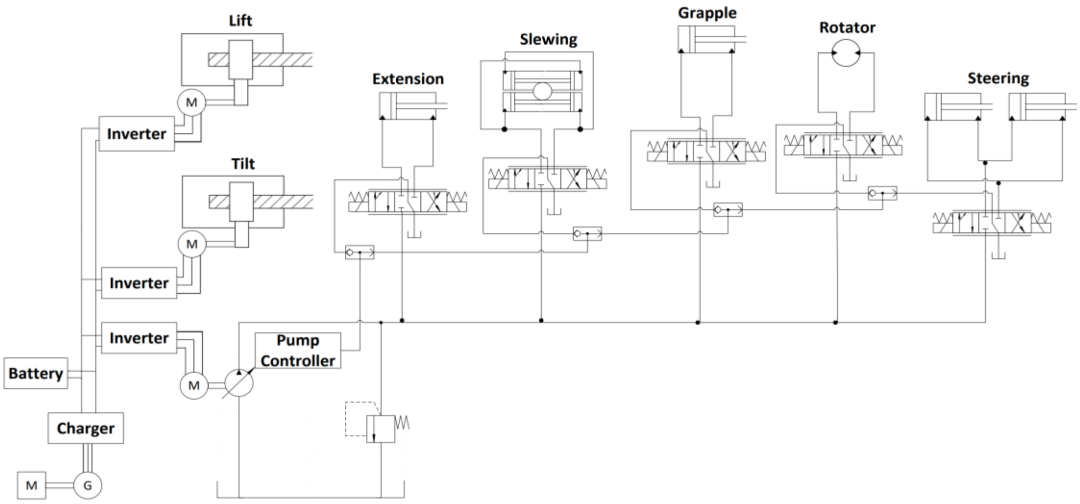

2.1.2 Excavator

An excavator is an NRMM used for a variety of operations which involve digging, lifting, and material handling in various earthmoving and industrial applications. In conventional excavators, these operations are primarily achieved using hydraulic actuators powered by LS hydraulics and controlled using throttling valves. Since the operation of an excavator is more versatile and hence involves all actuators intensively, for this study, all the major linear actuators are replaced with EMA. It shall be noted that the model is based on a 20-ton class backhoe excavator using two parallel-connected boom actuators. The system topology is shown in fig. 4, where two boom lift actuators, an arm actuator, and a bucket actuator are replaced with EMAs. The only major hydraulic component unchanged is a hydraulic motor used for the swing motion, as the focus of the current study is linear actuators.

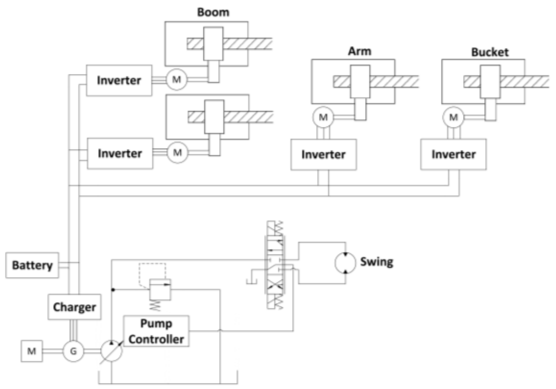

Figure 4: Schematic of EMA-based topology of the excavator

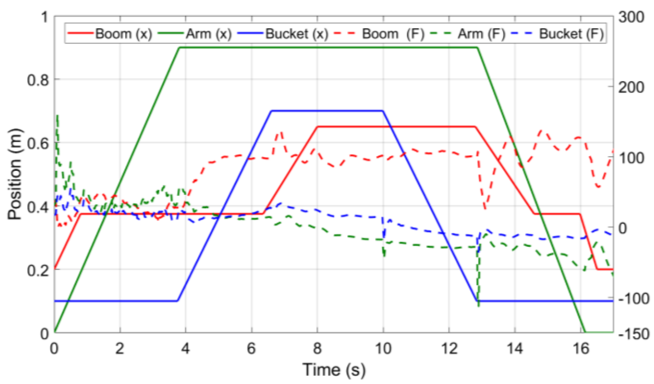

Figure 5: JCMAS duty cycle of the excavator

An excavator performs a wide variety of operations, and unlike the previous case of the forwarder, it is not possible to generalize its duty cycle. Hence, a standard digging cycle widely recommended for measurements of fuel consumption is used [22, 23]. The duty cycle, commonly referred to as JCMAS digging cycle is modified by creating load force in the bucket by using Mevea native earth model. The cycle position trajectory and the resulting load force for lift, tilt, and bucket actuators are illustrated in fig. 5.

2.1.3 EMA model

Electro-mechanical actuator (EMA) converts electrical energy directly to mechanical work, using gears and some mechanism such as ball screw or roller pitch [24]. This effectively eliminates the throttling and transmission losses which are inherently present with hydraulic actuators, giving them superior efficiency as compared to its hydraulic counterparts [25]. The EMA considered in this study uses a screw mechanism to convert the rotary motion of EM to linear motion. A simulation model of the permanent-magnet synchronous motor (PMSM) and the linear transmission mechanism are developed within the MATLAB/Simulink environment. The model is represented by the following equations.

The dynamics of the electric motor are derived from the fundamental principles governing its electrical and mechanical behavior. The electrical part of the model is described by voltage equations (1) and (2):

$$u_d = R_s i_d + L_d \frac{di_d}{dt} - \omega_s L_q i_q, \tag{1}$$

$$u_q = R_s i_q + L_q \frac{di_q}{dt} + \omega_s (L_d i_d + \Psi_r), \tag{2}$$

where R_s is the stator resistance, which may be considered identical for both the d- and q-axes. The parameters L_d and L_q are the d- and q-axis inductances, ω_s is the electrical rotor speed, and i_q and i_d are the stator currents. The rotor flux linkage along the d-axis, denoted as Ψ_r, is a constant. The flux linkage along the q-axis is assumed to be zero. [26]

As inverter tries to keep current i_d at zero, the output torque of the motor is modelled according to equation (3)

$$\tau_{EM} = K_t i_q - b_{EMA}\omega, \tag{3}$$

where b_{EMA} is the viscous friction coefficient and K_t is the motors torque constant. The force is calculated from the torque produced by the EM according to equation (4)

$$F_{EMA} = \frac{p}{2\pi} N \tau_{EM}, \tag{4}$$

where p is the pitch of the linear transmission and N is the gear ratio of the reduction gear between EM and linear transmission. The EMA output force F_{EMA} is then used as input in the mechanical model realized in Mevea simulation environment.

The main parameters used in the aforementioned equations are sourced from publicly available datasheets of commercial products [27, 28]. The primary objective of the current study is to propose the methodology for the selection of the EMA, as described earlier. Hence, the parameters used are solely for the example calculations for the present study. It is worth noting that the said parameters need to be changed according to the available products.

3 Actuator selection algorithm

The actuator selection algorithm is a high-level MADM algorithm that includes multiple subtasks, outlined in this chapter. It takes as input the data of the intended system's duty cycle, actuator characteristics, evaluation criteria including their relative importance, and design constraints. Based on these inputs and constraints, the algorithm suggests the optimal actuator from the set of alternatives. It uses AHP to model the MADM problem and rank the alternative EMAs. After that, the OP scaling algorithm is used to evaluate the selected aggregates. A flowchart of the selection process is shown in fig. 6, whereas the individual sub-tasks are described in the following sub-sections.

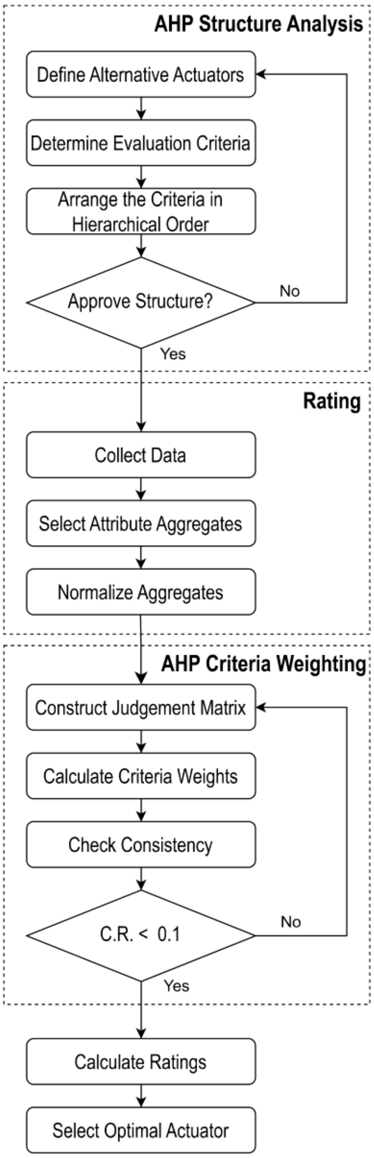

Figure 6: Flowchart of the selection algorithm

The first sub-task of the actuator selection algorithm is the structure analysis of the decision-making process. This involves defining the actuators to be compared, determining the evaluation criteria, and organizing them into a hierarchical structure, which defines the utility function form for the decision-making model. The hierarchical model follows the structure used in AHP.

The rating sub-task involves defining the actuator's duty cycle and collecting force and velocity data during this cycle for an example actuation system. The duty cycle data is then used to evaluate and normalize the aggregates in the decision-making model, with normalization based on reference values provided by the decision maker (DM). To assess each actuator alternative under its specific force and velocity constraints, the OP scaling algorithm is used. This algorithm scales down unreachable operating points due to lower force or velocity limits, estimating OPs for each actuator during the duty cycle.

The objective of criteria weighting sub-tasks is to rate the importance of utilities of sub-criteria $u_j(x_j)$ such that the total utility function U approximates the preference function P, an imaginary function describing DMs preferences ideally, as the following equation describes.

$$\nabla_{\mathrm{x}} U(X) = \nabla_x P[F(X)]. \tag{5}$$

The AHP framework is used to approximate the preference functions gradient by systematically rating the importance of the criteria. Ultimately, the Actuator Selection Algorithm rates the utility of each alternative actuator, with the total utility indicating the actuator's suitability for the given application in the compared machine.

3.1 Analytic Hierarchy Process

The analytic hierarchy process (AHP) is a systemic decision-making framework that facilitates complex MADM by breaking down a problem into smaller, more manageable components [29]. AHP employs pairwise comparisons to assess the relative importance of criteria, allowing for an intuitive and structured approach to decision making.

The process is built on a hierarchical structure that typically consists of three levels: the overall goal at the top, the criteria for evaluation in the middle, and the alternatives at the bottom, as shown in fig. 7 [29].

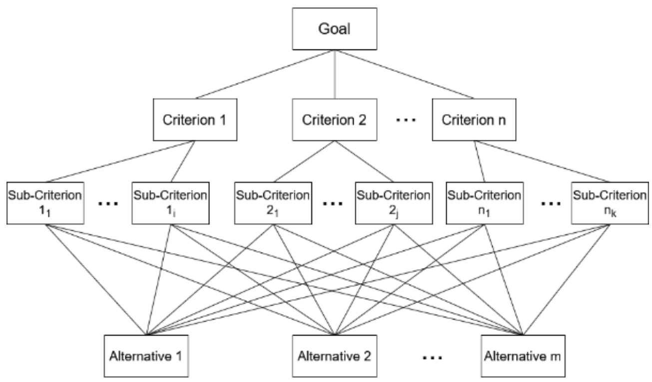

Figure 7: General structure of the hierarchy

The main steps of the AHP are as follows:

1. Define the problem and structure the hierarchy.
2. Conduct pairwise comparisons using a judgment matrix.

3. Calculate the consistency ratio (C.R.) to ensure judgment consistency.
4. Derive and normalize the priority vector.

Once the hierarchy is structured, the utility function modelling the decision makers preferences can be derived as follows,

$$U(X) = \sum_{j=1}^{n} \overline{w}_j u_j(x_j), \tag{6}$$

where $u_j(x_j)$ is the normalized utility aggregate of an attribute j and $\overline{w}_j$ is the weight of that attribute [30, 31].

Once the problem hierarchy has been defined, a comparative judgment of the criteria is performed. The relative importance of two criteria is compared on a scale from 1 to 9 in the judgment matrix, where 1 is least important and 9 is most important criteria.

If there is a set of n criteria (C), the judgment matrix A is formed as an $n\ x\ n$ matrix, $A = [a_{i,j}]$, where i,j ∈ {1, 2, …, n}. In the judgment matrix, the relative importance of criterion C_i compared to criterion C_j is represented by the element $a_{i,j}$ [17]. When $i = j$, the value of $a_{i,j}$ is 1, as a criterion is equally important when compared to itself. Additionally, the matrix is reciprocal, meaning that $a_{i,j} = 1/a_{j,i}$.

Matrix A is considered consistent if $a_{i,k} = a_{i,j} \cdot a_{j,k}\ \forall i, j, k \in \{1,2, \ldots, n\}$ [29]. This condition typically holds only in cases where the relative importance values are derived from exact measurements.

In the case of exact measurements, where the precise relative importance of different criteria is known, the elements of the judgment matrix A can be expressed as $a_{i,j} = w_i/w_j$, where w_i represents the priority of the criterion C_i. The judgment matrix A can then be written as [17]

$$\mathrm{A} = \begin{bmatrix} \frac{w_1}{w_1} & \frac{w_1}{w_2} & \cdots & \frac{w_1}{w_n} \\ \frac{w_2}{w_1} & \frac{w_2}{w_2} & \cdots & \frac{w_2}{w_n} \\ \vdots & \vdots & \ddots & \vdots \\ \frac{w_n}{w_1} & \frac{w_n}{w_2} & \cdots & \frac{w_n}{w_n} \end{bmatrix} \tag{7}$$

For a consistent matrix, the priority vector w is an eigenvector as well as priority vector of A, and the eigenvalue decomposition satisfies the equation

$$Aw = nw. \tag{8}$$

In practical applications, however, it is often impossible to determine the exact relative importance of criteria. Instead, the relative importance values are estimated, introducing some inconsistency into the judgment matrix. In such cases, the following approximation is used

$$A'w' = \lambda_{max} w', \tag{9}$$

where A' is perturbation of A and λ_{max} is the largest eigenvalue of the matrix A'. The closer λ_{max} is to n, the more consistent the matrix is. The consistency of A' may be examined by calculating the consistency index ($C.I.$) for A'

$$C.I. = \frac{\lambda_{max} - n}{n - 1}. \tag{10}$$

The $C.I.$ is then compared to random index $R.I.$ to obtain the consistency ratio $C.R.$, a relative measure of consistency

$$C.R. = \frac{C.I.}{R.I.}. \tag{11}$$

The random consistency index R.I. is the average C.I. calculated for randomly generated same-dimension judgment matrices. Average random consistency indices are presented in table 1 according to different dimensions of A [28].

Table 1: Average random consistency index

n	1	2	3	4	5	6	7	8
R.I.	0	0	0.52	0.89	1.11	1.25	1.35	1.40

The normalized criteria weights $\overline{w}$ are then derived from the elements of λ_{max}

$$\overline{w} = \frac{w}{\sum_{i=1}^{n} w_i}. \tag{12}$$

As a result of this process, the priority vector $\overline{w}$ is obtained, representing the weights of each criterion. These weights can then be used to rank the alternatives and identify the most suitable option.

3.2 Operation Point (OP) Scaling Algorithm

The OP scaling algorithm is used for predicting the operation points of alternative EMAs with differing maximum force and velocity constraints for a set task from single measurement of the intended duty cycle. The measured cycle may be seen as the power demand for the actuator and the algorithm tries to estimate where the operating points are located when the device's force or velocity capacity is exceeded in the original dataset.

As inputs from the measured duty cycle, the algorithm uses force F, velocity v, and gravitational load force component F_0, together with the maximum force constraint of studied actuator F_{max}. An example force constraint curve is depicted in red in fig. 8.

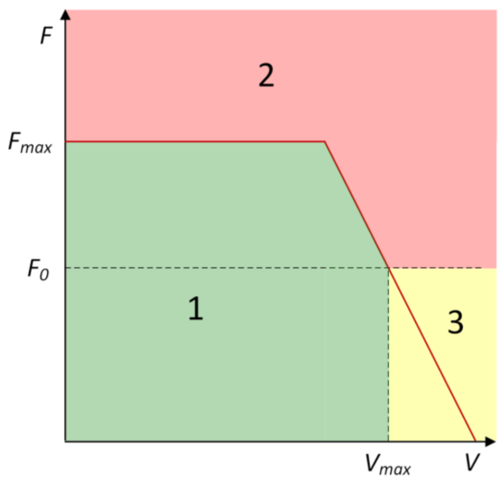

Figure 8: Example of force limit of actuator and operation point categorization

The measured operation points are reflected on the first quadrant and then divided into three categories by their location on the force-velocity graph:

1. Reachable operating points (Green).
2. Unreachable operating points constrained by maximum force (Red).
3. Unreachable operating points constrained by maximum velocity (Yellow).

The reachable operating points are not constrained by the force and velocity constraints; thus operating points inside area 1 are transferred into the set of scaled operating points unchanged.

The operating points constrained by maximum force are mapped on the force constraint curve such that the work done in one timestep into the system is equal for both; the measured and the scaled down operation points. For mapping these, similar force dynamics are assumed. The resulting scaled down operation points will have variable timesteps in order to compensate for the different force constraint and therefore, lower instantaneous power level. The steps of the algorithm for OPs in unreachable operating points constrained by maximum force (area 2) are graphically presented in fig. 9.

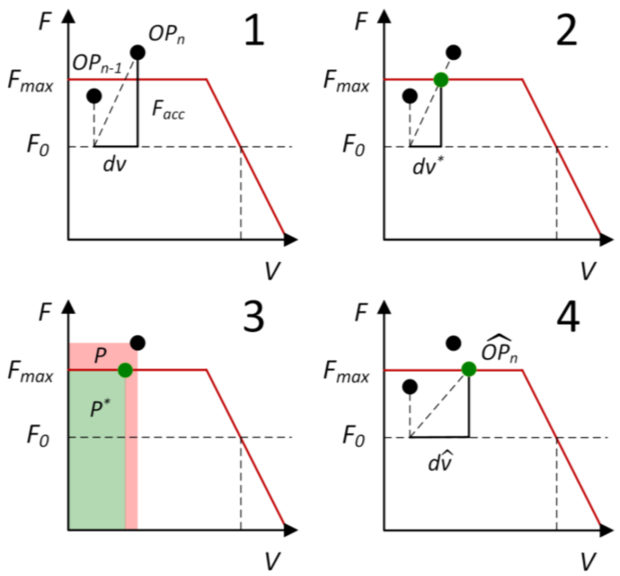

Figure 9: Steps of OP scaling algorithm for OPs in unreachable operating points constrained by maximum force

The algorithm assumes that the measured system follows the following finite difference approximation of the kinematic equation,

$$\frac{v(n)-v(n-1)}{\Delta t} = m_{eq}(n) \cdot F_{acc}(n), \tag{14}$$

where v is the velocity value of the operating point from measured dataset, Δt is the sampling time of measurement, and F_{acc} is the accelerating component of the force at actuator rod. The algorithm estimates the equivalent mass $m_{eq}(n)$ during one timestep, by solving gradient $k(n) = \Delta t \cdot m_{eq}(n)$ from the equation (14) depicted in step 1 of fig. 9 with formulae

$$k(n) = \frac{v(n)-v(n-1)}{F_{acc}(n)}. \tag{15}$$

Assuming that the difference in velocity is directly proportional to the accelerating component of force, the difference in velocity dv^* after the sampling time with the force constraint F_{max} is given by (fig. 9 step 2) the following formulae

$$dv^*(n) = k(n)\left(F_{max}\big(\hat{v}(n-1)\big) - F_0(n)\right). \tag{16}$$

After the original sample time Δt, the alternative actuator has done a different amount of work into the system compared to the actuator used for the measurement, thus, to end up at equal state energetically the new force must be applied for longer time. The following relationship between power and time can be established if the actuators output equal amount of energy.

$$\frac{\Delta\hat{t}(n)}{\Delta t} = \frac{P(n)}{P^*(n)} = \frac{v(n)F(n)}{\big(\hat{v}(n-1)+dv^*(n)\big)\,\hat{F}(n-1)}, \tag{17}$$

where $\Delta\hat{t}$ denotes the new timestep between scaled down operating points n and $n-1$, $\hat{v}$ and $\hat{F}$ are the velocities and forces of scaled down operating points, respectively. Whereas P and P^* are output powers of measured and scaled down actuators, respectively at a measurement sampling time of Δt after $n-1$ sample (fig. 9 step 3). The new velocity after the new time step $\Delta\hat{t}$ can be calculated as (fig 9 step 4)

$$d\hat{v}(n) = \frac{P(n)}{P^*(n)}\,k(n)\cdot\left(F_{max}\big(\hat{v}(n-1)\big) - F_0(n)\right) \tag{18}$$

and, therefore, the new scaled operating point is

$$\left[\hat{v}(n), \hat{F}(n)\right] = \left[\hat{v}(n-1) + d\hat{v}(n),\ F_{max}\big(\hat{v}(n-1)\big)\right]. \tag{19}$$

The operating points constrained by maximum velocity seen in fig. 8 are mapped on the maximum velocity border denoted by v_{max}, since for operation points with positive powers cannot cause additional increases in velocity as actuator in area 3 is not able to produce positive net force. For operation points with negative power values, the area 3 shall not be entered even though it is theoretically reachable due to risk of overrunning loads. Therefore, the OPs in area 3 are mapped on the velocity limit seen in fig. 8. Thus, the scaled OP is

$$\left[\hat{v}(n), \hat{F}(n)\right] = \left[v_{max}\left(F_0(n)\right), F(n)\right] \tag{20}$$

and the new time step between samples n and $n-1$ is

$$\Delta\hat{t}(n) = \frac{v(n)}{\hat{v}(n)}\Delta t. \tag{21}$$

The algorithm's estimated operation points and cycle time estimation were verified against simulation data of a 1 DOF crane realized in Simulink environment and the experimentally verified EMA model.

4 Algorithm Example Use Case: Forest Forwarder

This section demonstrates the use of the selection framework through an example. The goal is to optimize the combination of lift and tilt actuators by minimizing lifetime costs and load while maximizing productivity in a forest forwarder described in section 2.1.1. The PMSM servo motor rated power ranging from 3.2 to 11.6 kW, gear ratios of 3 and 7, and linear transmission screw pitch of 10, 15, and 20 mm are selected for the forest forwarder's lift and tilt cylinders using the actuator selection algorithm [25, 27]. This makes a total of 48 alternative EMA configurations for the machine, and in turn a total combination of 2304 (48x48) to select from. The main parameters of servo motors used in the selection are presented in table 2.

Table 2: The specifications of the servo motors used

	A	B	C	D	E	F	G	H
Rated Power (kW)	3.2	6.0	8.3	10.4	10.7	11.0	11.4	11.6
Rated Torque (Nm)	10	19	27	33	34	35	36	37
Stall Torque (Nm)	11	23	34	45	54	63	71	77
Peak Torque (Nm)	34	68	101	134	162	189	213	231

To evaluate the alternative actuators' productivity, the total load on the boom structure at the lift and tilt booms joint and the total investment cost were used as top-level criteria. These criteria were organized in the hierarchical structure shown in fig. 10.

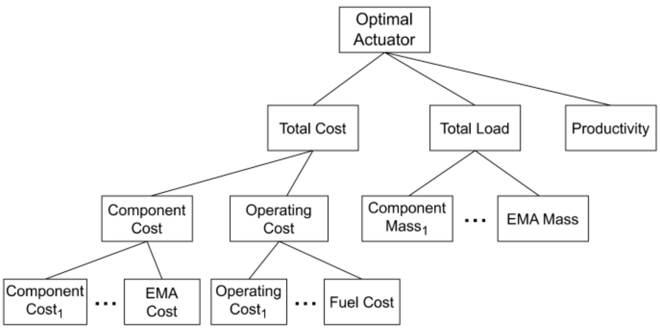

Figure 10: Hierarchy used in forest forwarder example

The fundamental idea of hierarchical modeling is to break the problem down into its elementary parts. The total load can be considered as the sum of all component masses connected to the boom. Similarly, the total cost can be divided into elementary cost components, some of which are influenced by the actuator selection. However, the forwarder's boom operation involves the simultaneous operation of multiple actuators. If a single actuator cannot complete its task in time, the cycle time increases directly. Therefore, this hierarchical approach does not apply to the productivity of the forwarder.

To evaluate the performance of each actuator alternative, the net present value of the investment cost, torque at the lift and tilt booms joint, and forwarder productivity are used. The duty cycle data for evaluation is generated using the simulation model of the forest forwarder. The collected data is input into the OP scaling algorithm, and the resulting operating points are used to calculate the fuel cost estimate during the duty cycle using the eq. (22). It shall be noted that all the values and numbers used in this example and results throughout are taken from the existing references [32, 33, 34]. Moreover, the actual values with respect to each machine case are presented in next section, focusing on results. The said values and numbers must be carefully considered for individual case. The cost calculations are as follows,

$$Cycle\ Cost = Cost_D \sum_n \left(\frac{\hat{v}(n) \cdot \hat{F}(n) \cdot \Delta\hat{t}(n)}{\eta_{EMA}\left(\hat{v}(n), \hat{F}(n)\right) \cdot \eta_I \cdot \eta_G} \right), \quad (22)$$

where $Cost_D$ is the cost of diesel per unit energy, the η_{EMA} represents the actuator's efficiency obtained from the EMAs efficiency map, η_I is the efficiency of the inverter, and η_G is the average efficiency of electric power generation from calorific value of diesel fuel. The total net present value of diesel consumption caused by the actuator over observation period used for evaluating the operation cost is,

$$NPV_{FC} = \sum_{y=0}^{y_{end}} Cycle\ Cost\ (Cycles/Year)\ (1 - k_D)^y, \quad (23)$$

where the k_D is the discount factor of future investments and y denotes the year when the cost occurs. For the component cost, public sources are used to estimate the servo motors cost, and the cost of the gear reduction system is set as constants for all alternatives.

If the productivity of the NRMM is defined as the time to complete a set duty cycle, cycle time can be used to evaluate it. To measure the productivity of an EMA alternative, the total estimated time to complete the duty cycle, as estimated by the OP scaling algorithm, is used. Since actuators work concurrently, the maximum increase in cycle time is considered at each time step.

$$t_{tot} = \sum_n \max\left(\Delta\hat{t}_{Lift}(n), \Delta\hat{t}_{Tilt}(n)\right). \quad (24)$$

The actuators' impact on the total load is estimated by EMA alternatives torque at the lift and tilt booms joint,

$$T_{EMA} = mean(d) \cdot m_{ema}, \quad (25)$$

where $mean(d)$ is the torque-inducing component of distance between the joint and actuator center of mass during the duty cycle and m_{ema} is the mass of the actuator alternative.

The thermal behavior of the servo motor is used as a constraint. The fulfilment of thermal constraint is assessed by the RMS value of the OP, which must be inside the nominal operating area of the motor to satisfy the constraint.

The aggregates are then normalized by reference values which are defined by the DM. The reference values are set for the duty cycle time t_{cycle}, the investment cost $Cost_{ref}$, and the mean torque at the lift and tilt booms joint during the duty cycle $mean(T_{Load})$.

Next, the criteria weights are determined using AHP, which evaluates the attribute weights w_j through pairwise comparisons between criteria. The pairwise comparison w_1/w_2 represents the ratio of partial differentials of the preference function relative to the aggregate values.

$$\frac{\frac{\partial P[F(X)]}{\partial x_1}}{\frac{\partial P[F(X)]}{\partial x_2}} \approx \frac{W_1}{W_2}. \tag{27}$$

To aid in assigning the values accurately in the AHPs pairwise comparisons, the normalization ranges with effect to utility between shared metric may be used if a known shared metric M_{12} exists of which gradient is,

$$\nabla_u M_{12}(u_1(x_1), u_2(x_2)) \approx \frac{\partial P[F(X)]}{\partial x_1} + \frac{\partial P[F(X)]}{\partial x_2}, \tag{28}$$

By evaluating the shared metric at the normalization points, the pairwise comparison can be calculated using formulae,

$$\frac{M_{12}(1,0) - M_{12}(0,0)}{M_{12}(0,1) - M_{12}(0,0)} = \frac{W_1}{W_2}. \tag{29}$$

The pairwise weight between productivity W_P and investment cost W_C is determined using a reference value for cost and an estimate for expected economic output based on typical forest forwarder values from the literature, as explained beforehand.

$$\frac{W_P}{W_C} = M_{PC} = \frac{NPV_{output}}{Cost_{ref}} \tag{30}$$

The pairwise comparison between total load and productivity is estimated based on the load's effect on machine productivity. While the load from the boom structure reduces productivity in a 1:1 relationship, the additional actuator mass also increases power consumption. Therefore, only a lower limit for the weight parameter can be estimated.

$$\frac{W_L}{W_C} \geq M_{LP} = 1. \tag{31}$$

For the pairwise importance between the remaining criteria, total cost, and total load, no suitable metric is found. With additional information, it may be possible to derive; however, for the example a consistent judgement matrix is assumed, and the weight parameter is solved from the already set weight factors. This assumption leads to a complete reliance on the previous weighting factors, and consistency of the judgement cannot be analyzed. Subsequently, weights of 1 are used between the different cost components.

5 Results

Based on the use case example presented in the preceding section, the EMA alternatives on both the machine cases are assessed. The following sub-sections present the results of forest forwarder and excavator cases. The results are represented as non-dominated solutions for the selection problem. A non-dominated solution is one where no objective can be improved without worsening another, thus representing an optimal trade-off. Solutions that are worse in all criteria compared to a non-dominated solution are excluded.

5.1 Forest Forwarder

For the actuator selection of the forwarder case, the following initial values were used, as presented in Table 3.

Table 3: Initial values used in forest forwarder actuator selection

Designation	Denotation	Value	Unit
$Cost_D$	Cost of diesel	$8.88\cdot10^{-8}$	€/J
t_{cycle}	Cycle time reference	41	s
-	Yerly operating time	2500	h
$Cost_{ref}$	Cost reference value	$1.08\cdot10^{6}$	€
NPV_{output}	Economic output	$1.76\cdot10^{6}$	€
y_{end}	Considered time	7	y
η_G	Engine-generator set efficiency	0.35	-
η_I	Inverter efficiency	0.95	-
k_d	Discount factor	0.1	-

Using the initial values, the following criteria weights are calculated $\overline{w}_C = 0.1701$, $\overline{w}_L = 0.5532$, and $\overline{w}_P = 0.2766$, where the factors are weights of total cost, total load, and total productivity, respectively. In the tilt function all PMSM alternatives fulfilled the RMS OP constraint unlike in the lift function, where out of the 8 PMSM alternatives only 5 (D-H) fulfilled the constraint using any effective transmission ratio.

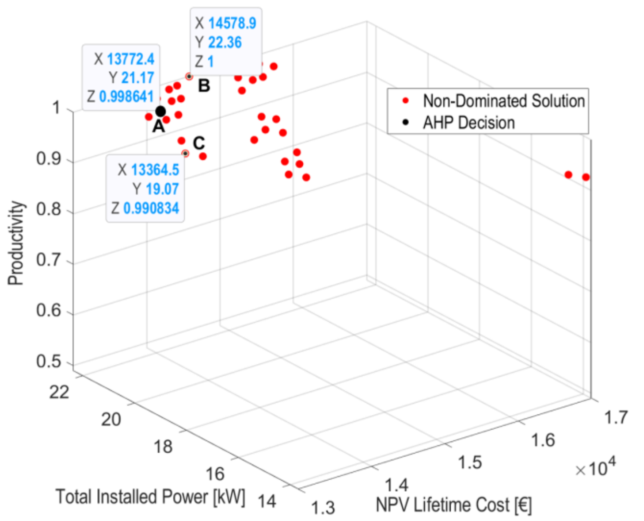

Figure 11: Non-dominated solutions for the forest forwarder

In fig. 11 productivity, total installed power and total investment cost values for all non-dominated lift and tilt actuator combinations are presented. Point A represents the optimal tradeoff given by AHP, based on weights defined here.

The A solution corresponds to a motor option with 10.7 kW nominal power using a gear ratio of 7 and a linear transmission pitch of 15 mm in the lift actuator, and in for the tilt actuator nominal power of 10.4 kW gear ratio of 3 and linear transmission pitch of 15 mm. Point B is the productivity maximizing solution at lowest lifetime cost. The solution B corresponds to 11.6 kW, 7 and 20 mm, and 10.7 kW, 3 and 15 mm for the lift and tilt cylinders nominal power, gear ratio and linear transmission pitch, respectively. Point C is a solution that minimizes the lifetime costs. It corresponds to 10.7 kW, 7 and 15 mm, and 8.3 kW, 3 and 15 for the lift and tilt cylinders nominal power, gear ratio and linear transmission pitch, respectively.

The results show that the lifetime costs of the system are higher than the lifetime costs for the productivity maximizing solution B for a large proportion of compared EMA combinations even with systems with lower component costs. This indicates that under-sizing the electric motor increases the lifetime costs of the system, which is explained by the lower efficiency of the EMA operating at higher velocities.

5.2 Excavator

In the excavator example use case the selection algorithm is used to select boom, arm and bucket cylinders resulting in 48^3 alternatives for the system, however only 6 (C-H) of the total 8 PMSM alternatives fulfilled the thermal constraint using any effective transmission ratio on the boom function. The selection hierarchy is applied as in the forest forwarder case, although the initial values—such as economic output and cost reference values—are updated using data from public sources [35, 36]. The adjusted initial values are presented in Table 4.

Table 4: Initial values used in excavator actuator selection

Designation	Denotation	Value	Unit
t_{cycle}	Cycle time reference	18	s
-	Yerly operating time	1800	h
DR	Duty Ratio	0.5	-
$Cost_{ref}$	Cost reference value	$3.71 \cdot 10^5$	€
NPV_{output}	Economic output	$5.64 \cdot 10^5$	€

Using the initial values, the following criteria weights are calculated: $\overline{w}_C = 0.1799$, $\overline{w}_L = 0.5468$, and $\overline{w}_P = 0.2734$, where the factors are weights of total cost, total load and total productivity, respectively. In fig. 12 the resulting non-dominated combinations for boom, arm, and bucket cylinders are presented. Point A represents the optimal trade-off determined by AHP based on the present weights. Solution A corresponds to 11.6 kW, 3 and 10 mm, 10.4 kW, 3 and 10 mm and 6.0 kW, 3 and 10 mm for the 2 boom, arm, and bucket cylinders' nominal power, gear ratio and linear transmission pitch, respectively. Point B maximizes productivity at the lowest lifetime cost. Solution B corresponds to 11.6 kW, 3 and 10 mm, 11.0 kW, 3 and 10 mm and 6.0 kW, 3 and 10 mm for the 2 boom, arm, and bucket cylinders nominal power, gear ratio and linear transmission pitch respectively. Point C minimizes lifetime costs. Solution C corresponds to 10.7 kW, 7 and 20 mm, 8.3 kW, 3 and 15 mm and 3.2 kW, 7 and 20 mm for the 2 boom, arm, and bucket cylinders' nominal power, gear ratio and linear transmission pitch respectively.

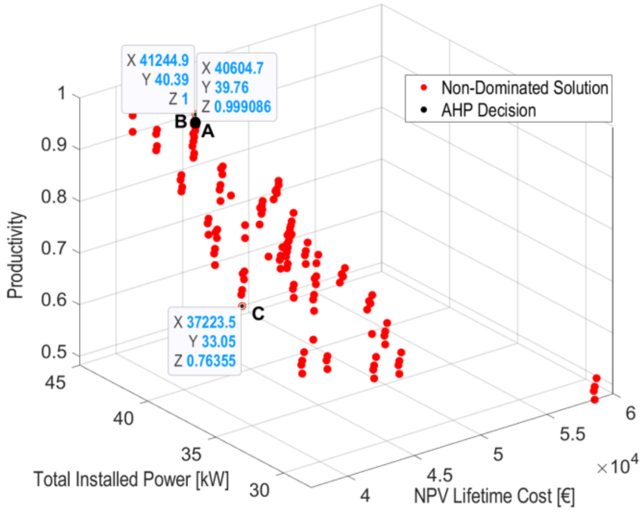

Figure 12: Non-dominated solutions for the excavator

In the excavator's case, a similar trend is seen where productivity tends to decrease as lifetime costs increase after point B. The selected actuation system is close to the productivity maximizing solution in terms of values selected for representation, however in the selection the mean position of the increased weight of the actuator is considered, thus on the mean load axis the difference between the points is greater.

6 Conclusion

In this paper, a multi criteria selection framework for selection of electro-mechanical actuators (EMA) for non-road mobile machinery is presented. In the framework operation points of actuator alternatives are estimated according to their force constraints using novel operation point (OP) scaling algorithm and an analytic hierarchy process (AHP) based Multi-Attribute Decision Making (MADM) algorithm to select the optimal actuator and the combination in machine.

As the case study, two NRMMs are used, a forest forwarder and an excavator. For the forwarder's lift and tilt functions, most of the alternative solutions evaluated exhibited a higher lifetime cost compared to the productivity-maximizing alternative, indicating how oversizing or undersizing can significantly affect costs. The best trade-off solution from the initial 2304 alternatives had nominal powers of 10.7 kW for the lift and 10.4 kW for the tilt, with respective gear ratios of 7 and 3, and linear transmission pitches of 15 mm each. By comparison, the excavator scenario produced 110,592 alternative configurations, where the best trade-off solution had nominal powers of 11.6 kW for the two boom actuators, 10.4 kW for the arm actuator and 6.0 kW for the bucket actuator, with gear ratios of 3, and linear transmission pitches of 10 mm for all actuators. The resulting non-dominated solutions for the excavator indicate that productivity tends to drop sharply when undersizing the actuators, showcasing the effect of higher utilization rate of each actuator in the measurement data on the productivity score.

These results indicate that optimizing one criterion often compromises another. Productivity emerges as a vital metric, as lifetime energy costs can outweigh initial investments. The chosen weights favor reduced lifetime costs and weight over minimal productivity losses, underscoring the importance of balancing multiple factors for EMA selection in NRMM.

In the future, more features can be added to the evaluation criteria. Particularly, thermal behavior should be included using the estimated OPs. Additionally, larger data samples should be utilized to ensure fully representative input data for decision-making, as there is a risk of over-optimization to match the performance needed for the input duty cycle. The applicability of input measurement data gathered from conventional hydraulically powered NRMMs should be tested. Unfortunately, such data was not available for this study. The concept is also extendable for electro-hydrostatic actuators (EHAs) with minor modifications, and with larger modifications, it can be studied for selecting between actuator technologies.

Acknowledgments

This research is a part of Business Finland project EMMA-2 (2471/31/2021). The authors gratefully acknowledge this funding and support by Business Finland.

References

[1] Casoli, P., Riccò, L., Campanini, F., & Bedotti, A. (2016). Hydraulic hybrid excavator - Mathematical model validation and energy analysis. Energies (Basel), 9(12), 1002-. https://doi.org/10.3390/en9121002

[2] XU, B., & CHENG, M. (2018). Motion control of multi-actuator hydraulic systems for mobile machineries: Recent advancements and future trends. Frontiers of Mechanical Engineering, 13(2), 151–166. https://doi.org/10.1007/s11465-018-0470-5

[3] Volvo CE unveils 100% electric compact excavator prototype. (2017, May 16). Volvo Construction Equipment. Retrieved February 13, 2025, from https://www.volvoce.com/global/en/news-and-events/news-and-stories/2017/volvo-ce-unveils-100-percent-electric-compact-excavator-prototype/

[4] Bahari, M., Paz, A., & Mattila, J. (2024). System-Level Performance Metrics Sensitivity of an Electrified Heavy-Duty Mobile Manipulator. IEEE Vehicular Technology Conference, 1–5. https://doi.org/10.1109/VTC2024-Fall63153.2024.10757845

[5] Qu, S., Fassbender, D., Vacca, A., & Busquets, E. (2021). A high-efficient solution for electro-hydraulic actuators with energy regeneration capability. Energy (Oxford), 216, 119291-. https://doi.org/10.1016/j.energy.2020.119291

[6] Heybroek, K. (2017). On Energy Efficient Mobile Hydraulic Systems: with Focus on Linear Actuation. https://doi.org/10.3384/diss.diva-142326

[7] Goswami, G., Tupitsina, A., Jaiswal, S., Nutakor, C., Lindh, T., & Sopanen, J. (2022). Comparison of Various Hybrid Electric Powertrains for Non-Road Mobile Machinery Using Real-Time Multibody Simulation. IEEE Access, 10, 107631–107648. https://doi.org/10.1109/ACCESS.2022.3213034

[8] Hu, X., Murgovski, N., Johannesson, L. M., & Egardt, B. (2014). Comparison of Three Electrochemical Energy Buffers Applied to a Hybrid Bus Powertrain with Simultaneous Optimal Sizing and Energy Management. IEEE Transactions on Intelligent Transportation Systems, 15(3), 1193–1205. https://doi.org/10.1109/TITS.2013.2294675

[9] Murgovski, N., Johannesson, L., Sjöberg, J., & Egardt, B. (2012). Component sizing of a plug-in hybrid electric powertrain via convex optimization. Mechatronics (Oxford), 22(1), 106–120. https://doi.org/10.1016/j.mechatronics.2011.12.001

[10] Silvas, E., Hofman, T., Murgovski, N., Etman, L. F. P., & Steinbuch, M. (2017). Review of Optimization Strategies for System-Level Design in Hybrid Electric Vehicles. IEEE Transactions on Vehicular Technology, 66(1), 57–70. https://doi.org/10.1109/TVT.2016.2547897

[11] Padovani, D., Dimitriou, P., & Minav, T. (2024). Challenges and solutions for designing Energy-Efficient and Low-Pollutant Machines in Off-Road hydraulics. Energy Conversion and Management. X, 21, 100526-. https://doi.org/10.1016/j.ecmx.2024.100526

[12] Xue, L., Wu, S., Xu, Y., & Ma, D. (2019). A simulation-based multi-objective optimization design method for pump-driven electro-hydrostatic actuators. Processes, 7(5), 274-. https://doi.org/10.3390/pr7050274

[13] Poole, A. D., & Booker, J. D. (2011). Design methodology and case studies in actuator selection. Mechanism and Machine Theory, 46(5), 647–661. https://doi.org/10.1016/j.mechmachtheory.2010.12.009

[14] Zhang, Y., & Cai, M. (2010). Mechanical Properties Evaluation for Pneumatic Actuator and Electric Actuator Based on AHP-FCE. 2010 WASE International Conference on Information Engineering, 3, 75–79. https://doi.org/10.1109/ICIE.2010.196

[15] Fassbender, D., & Minav, T. (2021). An algorithm for the broad evaluation of potential matches between actuator concepts and heavy-duty mobile applications. Actuators, 10(6), 111-. https://doi.org/10.3390/act10060111

[16] Yu, B., Wu, S., Jiao, Z., & Shang, Y. (2018). Multi-objective optimization design of an electrohydrostatic actuator based on a particle swarm optimization algorithm and an analytic hierarchy process. Energies (Basel), 11(9), 2426-. https://doi.org/10.3390/en11092426

[17] Saaty, T. L. (1980). The analytic hierarchy process : planning, priority setting, resource allocation. McGraw-Hill.

[18] Jiao, Z., Yu, B., Wu, S., Shang, Y., Huang, H., Tang, Z., Wei, R., & Li, C. (2019). An intelligent design method for actuation system architecture optimization for more electrical aircraft. Aerospace Science and Technology, 93, 105079-. https://doi.org/10.1016/j.ast.2019.03.048

[19] Mevea. (n.d.). Mevea. Retrieved February 12, 2025, from https://mevea.com

[20] Abid Abdul Azeez, Zakharov, V., Orifjonov, A., Niemelä, J., & Minav, T. (2022). Multi-physics Co-simulation of an Electric Reach Truck. In K. Schmitz (Ed.), The 13th International Fluid Power Conference (pp. 438-447). International Fluid Power Conference. https://doi.org/10.18154/RWTH-2023-04575

[21] Geiger, C., & Geimer, M. (2017). Efficiency optimisation of a forestry crane by implement hydraulics with energy recovery. VDI Berichte, 2017(2300), 175–184.

[22] Zhang, S., Minav, T., Pietola, M., Kauranne, H., & Kajaste, J. (2019). The effects of control methods on energy efficiency and position tracking of an electro-hydraulic excavator equipped with zonal hydraulics. Automation in Construction, 100, 129–144. https://doi.org/10.1016/j.autcon.2019.01.003

[23] Japan Construction Mechanization Association. (2007). Earth-moving machinery—Fuel consumption on hydraulic excavator—Test procedures. JCMAS H 020.

[24] Qiao, G., Liu, G., Shi, Z., Wang, Y., Ma, S., & Lim, T. C. (2018). A review of electromechanical actuators for More/All Electric aircraft systems. Proceedings of the Institution of Mechanical Engineers. Part C, Journal of Mechanical Engineering Science, 232(22), 4128–4151. https://doi.org/10.1177/0954406217749869

[25] Pustavrh, J., Hočevar, M., Podržaj, P., Trajkovski, A., & Majdič, F. (2023). Comparison of hydraulic, pneumatic and electric linear actuation systems. Scientific Reports, 13(1), 20938–20938. https://doi.org/10.1038/s41598-023-47602-x

[26] Krishnan, R. (2001). Electric Motor Drives: Modeling, Analysis, and Control. Prentice-Hall.

[27] UNIMOTOR FM - AC Brushless Servo motor. (n.d.). Nidec Corporation. Retrieved February 13, 2025, from https://cdn-static.nidec-netherlands.nl/media/3693-servomotoren-unimotor-fm-brochure-uk-iss13-0702-0032-13.pdf

[28] High performance actuator catalogue. (2025, January). EWELLIX. Retrieved February 13, 2025, from https://medialibrary.ewellix.com/asset/16172

[29] Saaty, T. L., & Vargas, L. G. (2012). Models, Methods, Concepts & Applications of the Analytic Hierarchy Process (2nd ed. 2012, Vol. 175). Springer Nature. https://doi.org/10.1007/978-1-4614-3597-6

[30] Marler, R. T., & Arora, J. S. (2010). The weighted sum method for multi-objective optimization: new insights. Structural and Multidisciplinary Optimization, 41(6), 853–862. https://doi.org/10.1007/s00158-009-0460-7

[31] Herrmann, J. W. (2015). Engineering decision making and risk management (1st ed.). Wiley. ISBN: 9781118919330

[32] Malinen, J., Laitila, J., Väätäinen, K., & Viitamäki, K. (2016). Variation in age, annual usage and resale price of cut-to-length machinery in different regions of Europe. International Journal of Forest Engineering, 27(2), 95–102. https://doi.org/10.1080/14942119.2016.1171964

[33] Eriksson, M., & Lindroos, O. (2014). Productivity of harvesters and forwarders in CTL operations in northern Sweden based on large follow-up datasets. International Journal of Forest Engineering, 25(3), 179–200. https://doi.org/10.1080/14942119.2014.974309

[34] Dvořák, J., Jankovský, M., Chytrý, M., Nuhlíček, O., Natov, P., Kormanek, M., & Löwe, R. (2021). Operational costs of mid-performance forwarders in czech forest bioeconomy. Forests, 12(4), 435-. https://doi.org/10.3390/f12040435

[35] Excavator Total Cost of Ownership Calculator. (n.d.). A Volvo Construction Equipment Blog. Retrieved February 13, 2025, from https://volvoceblog.com/tco-calculator/

[36] McGrillen, C. (2017). Case Study: Diesel Excavators Compared to Hybrid Excavators.